Current Applied Physics 84 (2026) 119–129

Contents lists available at ScienceDirect

Current Applied Physics

journal homepage: www.elsevier.com/locate/cap

Effect of LSPR, temperature and electric field on reduction of CO_2 in H_2O vapor using photocatalytic TiO_2-nanowires with Ag nanoparticles extruded from Ag-Nb-N-O film

Larisa Sorokina [a,*], Andrey Tarasov [a], Daria Dronova [a], Alexey Trifonov [a,b], Sergey Itskov [a], Aleksey Tregubov [c], Ekaterina Zhurina [c], Hanna Bandarenka [d], Sergey Dubkov [a], Dmitry Kozlov [c], Dmitry Gromov [a,e,**]

[a] Institute of Advanced Materials and Technologies, National Research University of Electronic Technology MIET, Bld. 1, Shokin Square, Zelenograd, 124498, Moscow, Russia
[b] National Research Centre "Kurchatov Institute", 1 Kurchatov Square, 123182, Moscow, Russia
[c] S.P. Kapitsa Scientific Technological Research Institute, Ulyanovsk State University, 42 Leo Tolstoy Street, 432017, Ulyanovsk, Russia
[d] Applied Plasmonics Laboratory, Belarusian State University of Informatics and Radioelectronics, 6 Brovka St., 220013, Minsk, Belarus
[e] Institute for Bionic Technologies and Engineering, I.M. Sechenov First Moscow State Medical University, Bolshaya Pirogovskaya 2, 119435, Moscow, Russia

ARTICLE INFO

Keywords:
TiO_2 nanowires
Localized surface plasmon resonance
CO_2 photocatalysis

ABSTRACT

This paper reports on the formation and study of Ag-Nb-N-O/TiO_2 nanowires (NWs) for photocatalytic reduction of CO_2. Firstly, the Ag-Nb-N-O thin film was grown by simultaneous magnetron sputtering of Ag and Nb targets in an atmosphere of Ar and N_2. Subsequently, the Ag-Nb-N-O thin film was coated with TiO_2 NWs, which were presynthesized by a hydrothermal method and then annealed at 500 °C. Before photocatalytic tests, the Ag-Nb-N-O/TiO_2 NW samples were subjected to heat treatment at 350 °C. A morphology of the fresh and 350 °C-annealed Ag-Nb-N-O/TiO_2 NWs was comprehensively studied by SEM, TEM, EDXS, and XRD. Heating was found to facilitate the extrusion of Ag particles from the bulk of the Ag-Nb-N-O film to its surface. In addition, the heat treatment led to partial evaporation of silver and its further redeposition on the surface of TiO_2 NWs in the form of Ag nanoparticles. The Ag-Nb-N-O/TiO_2 NWs subjected to the 350 °C heating possessed a remarkable photocatalytic activity in the synthesis of methanol from CO_2, which was 3 times over that of the pure TiO_2 NWs. This is associated with the contribution of localized surface plasmon resonance of Ag particles to generation of the charge carriers. Moreover, we demonstrate that LSPR-induced heating of Ag nanoparticles, confirmed by IR imaging, plays a crucial role in charge carrier separation. The thermoelectromotive force generated by the temperature gradient facilitates electron transfer from TiO_2 to Ag, thereby improving CO_2 reduction efficiency. Additionally, we revealed that an external electric field enables an improvement of the Ag-Nb-N-O/TiO_2 NW photocatalytic activity providing an additional increase in the methanol yield by 60 %.

1. Introduction

In-depth understanding of photocatalytic processes in semiconductor compounds has been highly demanded in many areas of human life including but not limited to the purification of water [1–3] and air [4–6], engineering of self-cleaning coatings [7,8], decomposition of organic pollutants [9,10], and production of fuel by decomposing water into hydrogen and oxygen [11,12]. The photocatalysis mechanism relates to photogeneration of charge carriers upon absorption of incident light with a photon energy over the width of the semiconductor band gap. All these processes are associated with the high oxidizing capacity of photocatalysts. However, photocatalysts are also capable of carrying out reduction, a process that is a reverse of oxidation. For example, they can reduce CO_2 from air in presence of water to a series of hydrocarbons [13–15]. One of the most well-known and applied semiconductor photocatalysts is titanium oxide (TiO_2).

* Corresponding author.
** Corresponding author. Institute of Advanced Materials and Technologies, National Research University of Electronic Technology MIET, Bld. 1, Shokin Square, Zelenograd, 124498, Moscow, Russia.
E-mail addresses: larasork@gmail.com (L. Sorokina), gromadima@gmail.com (D. Gromov).

https://doi.org/10.1016/j.cap.2026.01.001
Received 22 July 2025; Received in revised form 30 December 2025; Accepted 4 January 2026
Available online 5 January 2026

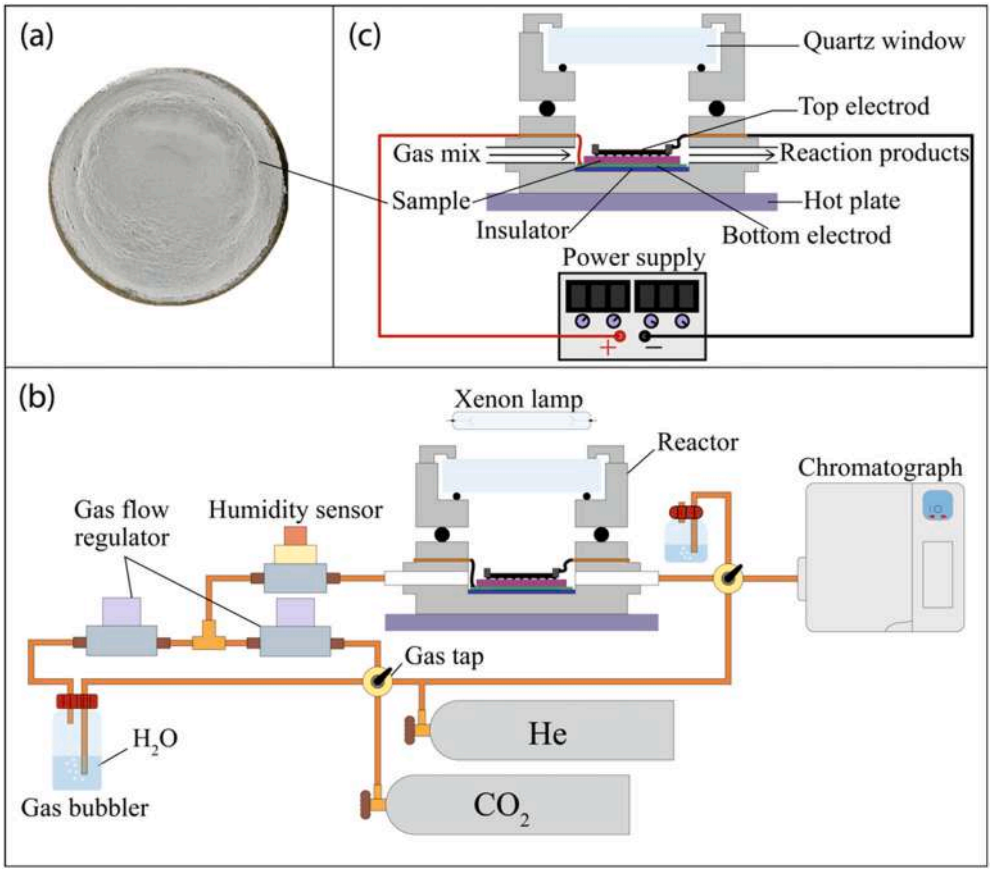

Fig. 1. (a) General view of the sample; (b) diagram of the measuring stand; (c) diagram of the photocatalytic reactor.

Photocatalytic properties depend a lot on the specific surface area [16,17], crystalline phase [18,19], and lifetime of charge carriers [20,21]. These parameters are often defined by morphology of the semiconductor nanostructures. In particular, TiO_2 structures can have several crystalline modifications yet many variations in morphologies. They can be divided into 0D – nanoparticles and nanospheres [22,23], 1D – nanowires and nanotubes [24,25], and 2D – thin films and nanosheets [26]. The 0D structures have a high specific surface area but are characterized by a low charge carrier mobility due to severe defectiveness. An opposite situation is observed in the 2D structures, which have a relatively small specific surface area but a higher charge carrier mobility. Thereby, the 1D structures occupy an intermediate position between the 0D and 2D structures providing a specific research interest to them [27]. Having a relatively large specific surface area, the 1D structures possess a fairly high mobility of charge carriers along the axial direction [28,29]. The long length and nearly perfect crystallinity of nanowires (NWs) help to reduce recombination probability and promote diffusionless transfer of charge carriers [28,29]. Our recent study [30] demonstrated the better CO_2 reduction capability on TiO_2 NWs compared to the commercial TiO_2 P25 powder with the similar phase composition.

An improvement of photocatalytic activity can be provided by modification of TiO_2 nanomaterials with metal particles to create a metal/semiconductor (M-S) heterostructure. Metals in such structures can play a dual role of a co-catalyst due to their own photocatalytic activity, participating in the photocatalysis process, and traps for electrons, which increases the lifetime of charge carriers [31,32]. In these terms, the heterostructures with plasmonic metals are even more prospective for photocatalysis application [33]. Local surface plasmon resonance (LSPR) in plasmonic particles provides an efficient absorption of the radiation at a target wavelength range [34], a generation of "hot" charge carriers, processes of plasmon resonance energy transfer [35,36], and a local heating [37,38]. The M-S interfacing leads to the formation of a Schottky barrier when the equilibrium Fermi level is established due to the difference in the work function of the electrons in metal and semiconductor. The LSPR effect causes generation of "hot" electrons and holes in plasmonic metal nanoparticles [39]. Due to the Schottky barrier, these charge carriers are separated by the M-S contact, which increases the efficiency of the redox reaction [40].

There are many ways to form metal particles on semiconducting substrates including physical [41–43], electrochemical [44,45], and chemical [46–51] methods. An original and promising technique is an extrusion of plasmonic structures from thin two- or multi-component films, where the plasmonic metal in the form of particles and nanoparticles is released from the alloy during external energy exposure [52–55]. An attractive feature of this approach is a protection of the plasmonic particles from an oxidation while they are combined with other components in the bulk of the alloy film [53].

An increase in photocatalytic activity is possible by applying an electric field. In particular, it was shown that upon an electric field of about 10^4 V/cm, CO appears as a product of the CO_2 reduction in the water vapor [56]. Moreover, it was revealed that an additional improvement of photocatalytic activity is achieved under the combined effect of various fields [57].

The aim of this work was to investigate a combined effect of light, temperature, and electric field on photocatalytic activity of the Ag-Nb-N-O/TiO_2 NWs heterostructure for the reduction of CO_2 in the water vapor. The photocatalytic activity was assessed by evaluating a yield of methanol as a result of the CO_2 reduction reaction in the water vapor. The reaction took place upon irradiating the structure with a xenon lamp light with simultaneous thermal heating, and application of an external electric field.

2. Materials and methods

In this work, the TiO_2 NWs and Ag-Nb-N-O/TiO_2 NWs samples were prepared on a 50-μm thick titanium foil of a 7 cm^2 area. The top view photos of the resulting samples are shown in Fig. 1 (a).

Before processing, the Ti substrates were ultrasonically cleaned in an isopropyl alcohol/acetone solution (50:50) for 30 min and rinsed in deionized water. Then, they were briefly etched in a $HF:HNO_3:H_2O$ (30:20:150) solution, rinsed again in deionized water, and dried in isopropyl alcohol vapor. A thin film of the $Ag_{51}Nb_{26}N_{17}O_5$ alloy with a thickness of about 250 nm was deposited on the Ti substrate by simultaneous magnetron sputtering of Ag and Nb targets in an atmosphere of Ar+10 vol% N_2 at a pressure of 0.6 Pa. The source of oxygen in the as-deposited film was the residual atmosphere.

TiO_2 NWs were formed by a hydrothermal method. In more detail, 50 mL of an aqueous 10 M NaOH solution was placed in a 100 mL autoclave and 0.6 g of commercial powder TiO_2 P25 (Evonik) was added. The solution was then stirred for 30 min on a magnetic stirrer. The prepared solution was placed in the autoclave and heated in a muffle furnace at a temperature of 250 °C for 9 h. Once the synthesis was completed, the autoclave was cooled to room temperature. The nanowires were transferred to a beaker containing 400 mL of deionized water and 50 mL of HCl. The solution was heated to 60 °C and stirred for 20 min. Then the nanowires were separated from the solution using vacuum filtration and washed repeatedly to neutral pH. After washing, the nanowires were dried in air at a temperature of 100 °C. The obtained nanowires were thermally treated at a temperature of about 500 °C for 4 h in air, since, as was shown earlier, this mode gave the best results of photocatalysis [30].

A formation of the TiO_2 NWs layer over the Ag-Nb-N-O alloy film on titanium substrates was carried out by the drop deposition method. For this purpose, a suspension was prepared consisting of 1.5 mL of deionized water and about 15 mg of TiO_2 NWs. The suspension was treated in an ultrasonic bath for 30 s to ensure uniform distribution of the nanowires in the solution. The suspension was then placed in a medical syringe and applied to a titanium foil with a layer of alloy. The spreading of the suspension was limited by a silicone ring with an internal diameter of about 30 mm. The substrates were heated to 85 °C on a heating table until the water completely evaporated.

Before studying the photocatalytic activity, the finished samples were annealed in a Project 1250/30 muffle furnace in an air atmosphere at a temperature of 350 °C for 60 min in order to form silver clusters and remove organic contaminants.

The photocatalytic activity of the samples was studied in a thermally stabilized flow reactor of a 25 cm^3 volume with a quartz window and two gas inlets. The diagram of the measuring stand is shown in Fig. 1 (b). The gas mixture of CO_2 and He was partially passed through a bubbler in such a way that the humidity of the gas mixture at the inlet of the reaction chamber was 60 %, which was controlled by a DV2TSM V humidity sensor (Fig. 1 (b)). The gas flow rate was set by a regulator and was 3 mL/min. A stainless-steel grid electrode with a wire diameter of 0.64 mm and a cell size of 1.92 mm was installed on top of the sample in the reactor to apply voltage (Fig. 1(c)). The Ti foil substrate, coated with an Ag-Nb-N-O film, was biased positively, while the top electrode, simply placed in contact with the TiO_2 NWs layer on top, was biased negatively. A constant voltage in the range from 0 to 200 V was applied between the electrodes. Prolonged exposure to voltages exceeding 200 V resulted in dielectric breakdown, during the measurements, which typically lasted several hours. The electrode spacing was determined by the thickness of the functional layer and was approximately 50 μm, resulting in an estimated electric field strength of up to $\sim 4 \times 10^6$ MV m^{-1} at the maximum applied voltage. The samples were irradiated using two 35 W xenon lamps. The measurements were carried out at a reactor temperature of 100 °C.

The products of the photocatalytic reaction were analyzed using a Crystal 5000 gas chromatograph equipped with an Agilent HP PLOT Q capillary column and a plasma ionization detector. The reaction products were determined by the release time. The concentration of the product was estimated based on the peak area. Before the measurement, the reactor was heated to 60 °C and purged for 1 h. Once after the sample was placed in the reactor, the release of products was recorded in the dark three times in a row. The obtained base values were subtracted during further calculation of the product yield. The first measurements of the photocatalytic activity of the sample were carried out under the influence of radiation only, and subsequent measurements were carried out under the influence of both radiation and an electric field. The final yield of the product in μmol/(g·h) was calculated using equation (1):

$$Yield\ (\mu mol\ /\ g \cdot h) = \frac{C(mg/m^3).Q(m^3/h)}{M(mg/\mu mol \cdot m(g)} \quad (1)$$

where C is concentration, Q is flow rate, M is molar mass and m is sample mass.

The morphology of samples was studied using a Helios G4 CX scanning electron microscope (SEM). The measurements were carried out at an accelerating voltage of about 5 kV and a current of 21 pA.

X-ray diffraction analysis (XRD) was performed on a Rigaku MiniFlex 600 diffractometer (Rigaku Corporation, Tokyo, Japan) with a Cu K_α radiation source ($\lambda = 1.5418$ Å). The Bragg angle 2θ range was 10°–60°.

Transmission electron microscopy (TEM) was used to investigate the structure of Ag-Nb-N-O alloy film and TiO_2 NWs. For the TEM-study, a 50 nm thick Ag-Nb-N-O film was deposited on a KCl salt crystal by magnetron sputtering. The resulting thin film was then separated from the crystal by immersion in deionized water and dissolution of the KCl salt. The film that floated to the surface was transferred to a copper grid for TEM. The samples were examined using a Tecnai G2 20 transmission electron microscope (FEI company, Hillsboro, OR, USA) with an accelerating voltage of 200 kV. The microscope was equipped with a high-angle annual dark field detector (HAADF) for operation in scanning mode and an EDAX energy-dispersive X-ray spectrometer (EDXS).

The diffuse reflectance spectroscopy (DRS) of the experimental samples was performed with a SF-56 (OKB SPECTR LLC, Saint-Petersburg, Russia) spectrometer, which provides measurements of the reflectance spectra in the range 290–1100 nm.

3. Results

In this work, an approach based on controlled elemental redistribution in multicomponent thin films was employed to form plasmonic Ag nanoparticles on the TiO_2 surface [52–55]. Similar phenomena, often referred to as phase separation, are well known in transition-metal alloy thin films during thermal treatment, where one component preferentially bonds with nitrogen (and oxygen, when present as an additive), while another surface-active component predominantly migrates toward an interface or the surface and either undergoes a chemical reaction there [58,59] or segregates in the form of a nanoparticle array [53,60].

Specifically, the selection of the Ag-Nb-N-O alloy components was guided by this mechanism and the criteria discussed in Ref. [59]. Accordingly, it was assumed that Nb, N, and O in the present system play a dual role: on the one hand, they enable controlled segregation of Ag at the film surface, and on the other hand, thermal treatment in air leads to the formation of an electrically insulating niobium oxynitride layer capable of sustaining relatively high electric field strengths.

3.1. TEM characterization of Ag-Nb-N-O thin film

Before the TEM analysis, the Ag-Nb-N-O thin film was annealed at a temperature of 350 °C for 60 min. This procedure was performed to extrude silver from the Ag-Nb-N-O thin film onto the surface and form an array of Ag particles on it. The mechanism of this process was described elsewhere [53]. The results of the TEM-study of these samples are shown

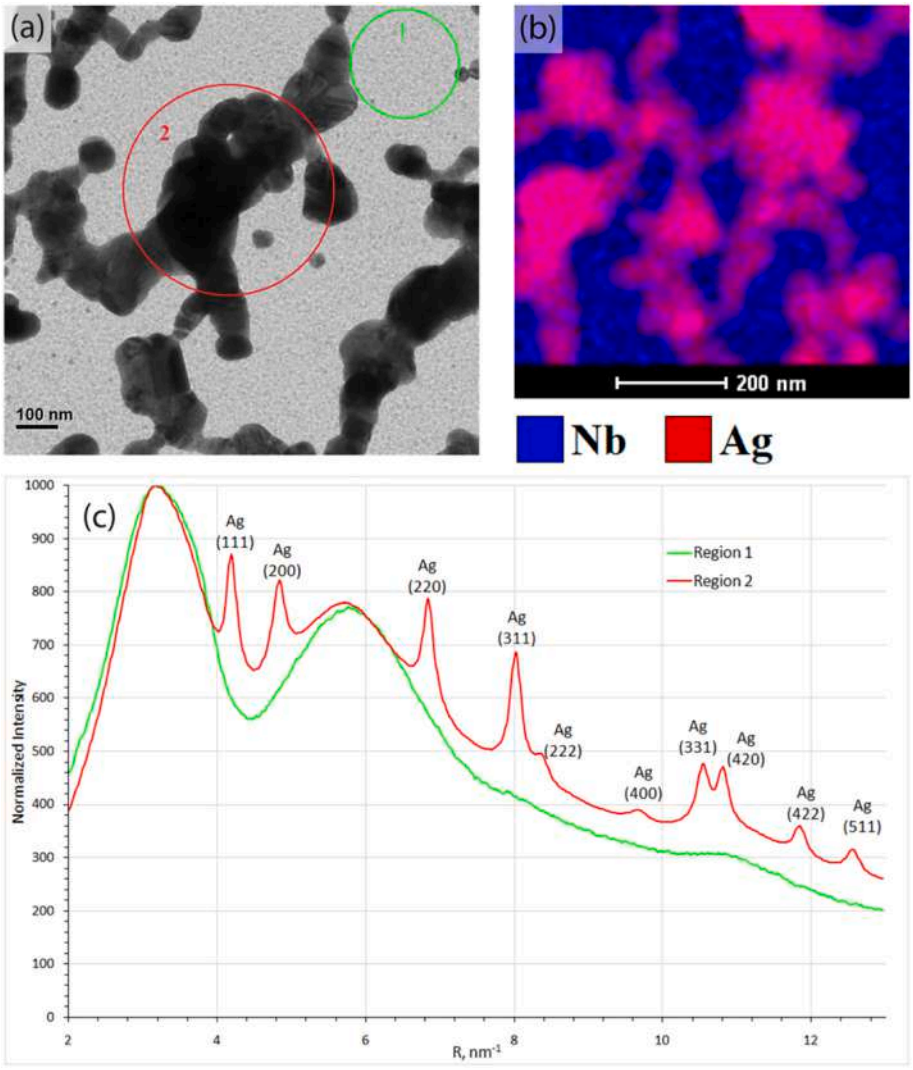

Fig. 2. Morphology characterization of Ag-Nb-N-O films: (a) TEM-image; (b) EDXS mapping; (c) SADP.

in Fig. 2.

Selected area diffraction patterns (SADPs) were obtained in two regions of the sample shown in Fig. 2 (a): region 1 contains only the base film and region 2 contains the film with particles. These results are presented in Fig. 2 (c) as a function of intensity versus distance from the center of the diffraction pattern. The diffraction pattern of region 1 has the form of diffuse rings, characteristic of amorphous materials (green curve in Fig. 2 (c)). In region 2, reflections from the face-centered cubic lattice of silver are superimposed on this pattern (red curve in Fig. 2 (c)).

Thus, the Ag-Nb-N-O structure after annealing at 350 °C represents polycrystalline silver particles on an amorphous niobium film.

3.2. TEM characterization of TiO_2 NWs

Fig. 3 (a) and (b) depict TEM-images of TiO_2 NWs. SADP (Fig. 3 (c)) looks like concentric rings typical for polycrystalline samples.

The SADP picture consists of reflections of two polymorphic phases of titanium oxide: anatase and monoclinic phase "bronze" (TiO_2-B). Crystallographic planes (001) and (310) of TiO_2-B crystallite are visible in the high-resolution image Fig. 3 (d).

3.3. SEM characterization

Figs. 4 and 5 show the SEM-images of the Ti-foil/TiO_2 NWs and Ti-foil/Ag-Nb-N-O/TiO_2 NWs samples at different magnifications, respectively. The sample shown in Fig. 5 was annealed at 350 °C.

Analysis of the SEM images showed that the nanowires synthesized by the hydrothermal method had a length from 6 to 10 μm and a thickness from 30 to 300 nm. The thickness of the layers was about 50 μm.

As it is seen in Fig. 5(b–d), Ag particles can already be found on the surface of the Ag-Nb-N-O alloy film. Average size of these particles is about 300 nm (Fig. 5 (c)). In most cases, the distance between the particles is very small (10–50 nm) but in some cases it reaches 500 nm. At a higher magnification (Fig. 5 (d)), one can see that the annealing at 350 °C caused partial redeposition of silver from the surface of the Ag-Nb-N-O film onto the TiO_2 NWs surface. As a result, Ag nanoparticles with a diameter of about 10–40 nm were formed. The Ag redeposition is additionally proved by the EDXS mapping presented in Fig. 5 (e). Signatures of the silver atoms (yellow) are distinguished in the regions with the Ti atoms (blue). The fact that silver evaporates easily at low temperatures has previously been demonstrated [61,62]. The EDXS mapping also shows that the sample surface area is covered with silver up to approximately 30 % (Fig. 5 (e)).

3.4. XRD characterization

Fig. 6 shows X-ray diffraction patterns of the TiO_2 NWs samples on

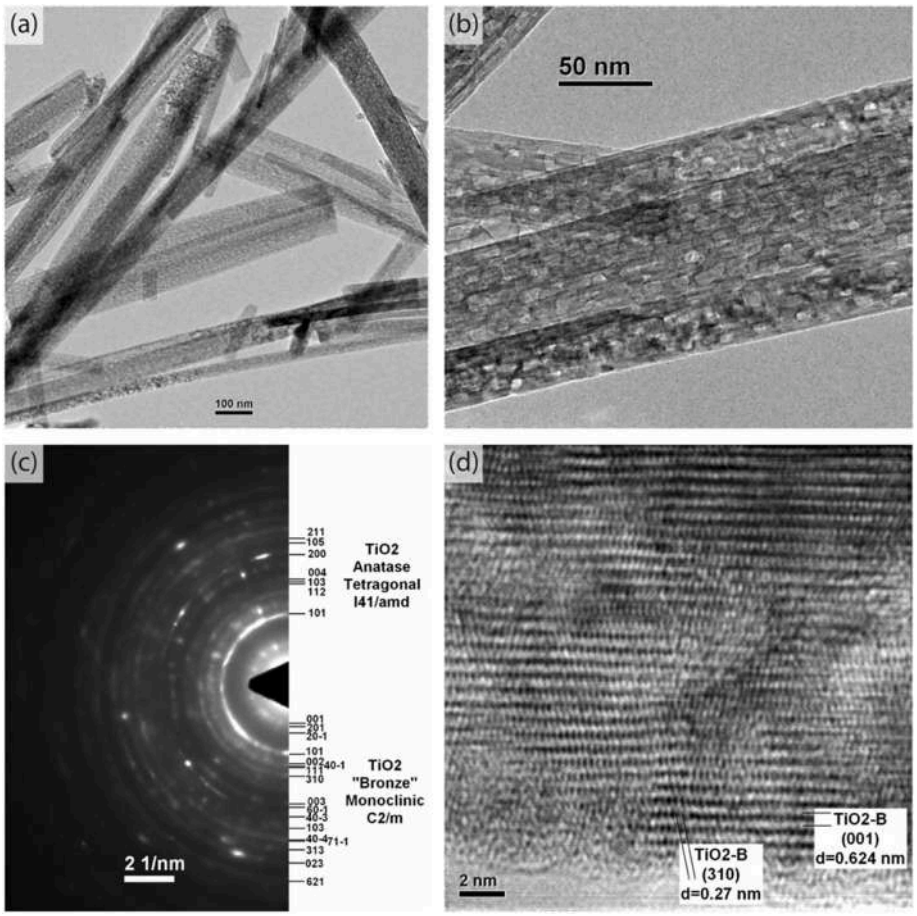

Fig. 3. Results of the TEM-study of the TiO_2 NWs annealed at a temperature of 350 °C: (a) powder image at a magnification of 1950 × ; (b) powder image at a magnification of 71k × ; (c) selected area diffraction pattern; (d) high-resolution image of a crystal at a magnification of 1050k × .

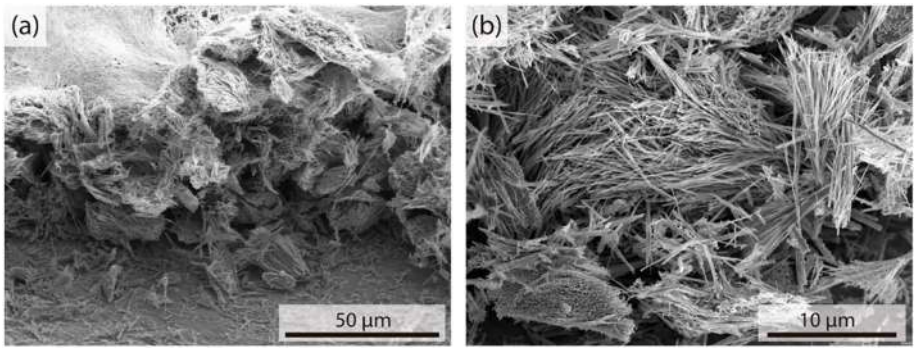

Fig. 4. SEM-images of the TiO_2 NWs layer profile on titanium foil at magnifications a)2400 × and b) 10k × .

the Ti foil with and free of a thin Ag-Nb-N-O film.

They contain characteristic peaks of titanium associated with the substrate foil. The remaining set of peaks belongs to the nanowires, which are a mixture of TiO_2-B, rutile and anatase phases. This is in a good agreement with the results reported before [30]. In the XRD pattern of Ag-Nb-N-O/TiO_2 NWs, low-intensity peaks of metallic Ag appear along with the same set of peaks as for the Ti-foil/TiO_2 sample (the peaks are not labelled to avoid the figure cluttering).

The dense array of Ag particles on the Ag-Nb-N-O/TiO_2 NWs sample formed after the heat treatment at 350 °C is a source of multiple “hot spots” in the plasmonic coating.

It also provides formation of more contact points between TiO_2 NWs and Ag particles. The multiplication of the TiO_2/Ag interface spots can potentially lead to charge transfer and local electric field enhancement of photocatalytic activity. It is generally accepted that the pure TiO_2 samples possess photocatalytic activity upon near ultraviolet (UV) exposure (approx. 365 nm) while the excitation light wavelength which induces photocatalytic activity in the Ag-modified TiO_2 samples, shifts to the visible range [63]. Thereby, we expect that the surface modification of TiO_2 NWs with Ag nanoparticles observed in Fig. 5 can additionally contribute into photocatalytic activity upon the Xe lamp exposure, which typically has more intensive spectrum in the visible range, in particular at 475 nm band.

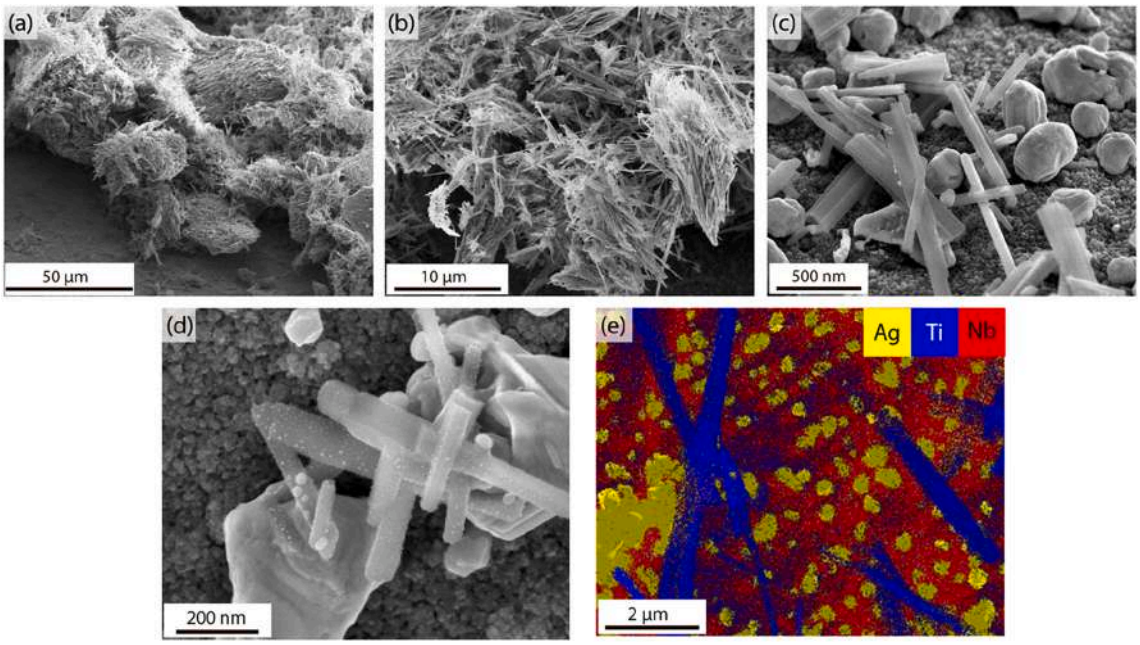

Fig. 5. Morphology characterization of the Ag-Nb-N-O/TiO_2 NWs sample after annealing at 350 °C: (a) SEM-image of TiO_2 NWs layer in profile; (b) SEM-image of TiO_2 NWs at a magnification of 10k × ; (c) SEM-image of TiO_2 NWs region with Ag particles; (d) SEM-image of the Ag-Nb-N-O/TiO_2 NWs at a magnification of 300k × where redeposited Ag nanoparticles are visible on the surface of TiO_2 NWs; (e) EDXS- map of TiO_2 NWs region with Ag particles on Nb film.

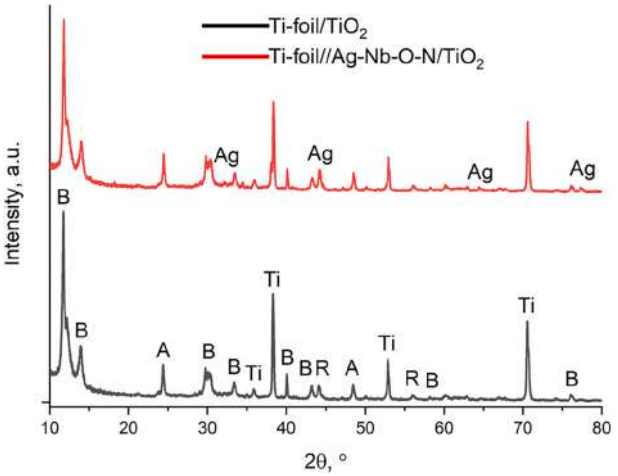

Fig. 6. Phase composition of TiO_2 NWs and Ag-Nb-N-O/TiO_2 NWs layers on Ti foil according to the X-ray diffraction data. Designations: Ti – titanium, A – anatase, R – rutile, B – bronze (TiO_2-B), Ag – silver.

3.5. Optical characterization of TiO_2 NWs and Ag-Nb-N-O/TiO_2 NWs

The dense array of Ag particles on the Ag-Nb-N-O/TiO_2 NWs sample formed after the heat treatment at 350 °C is expected to be a source of multiple "hot spots" in the plasmonic coating. Here, plasmonic properties of the silver-containing sample subjected to the heat treatment were studied in comparison with the pure TiO_2 NWs. We prepared the samples of TiO_2 NWs and Ag-Nb-N-O/TiO_2 NWs to collect their diffuse reflectance (DR) spectra depicted in Fig. 7.

The DR spectrum of Ag-Nb-N-O/TiO_2 NWs shows two bands at 325 nm and 427 nm associated with the light absorption in the sample. The rather sharp 321-nm band is also observed in the DR spectrum of TiO_2 NWs and characterizes optical absorption edge of titanium dioxide. On the other hand, the band around 450 nm is typical just for the silver-containing sample signifying about its plasmonic properties, i.e. LSPR effect has the highest intensity at this band. The LSPR band is broad enough and overlaps a range from ~360 nm to ~560 nm, which is caused by the size polydispersity of the Ag particles.

The DR spectra were used to determine the band gap energy of the samples following an approach reported elsewhere [64]. Fig. 7 (b, c) shows that the band gap energy of the TiO_2 NW sample corresponds to 2.9 eV but is modified down to approximately 2 eV during

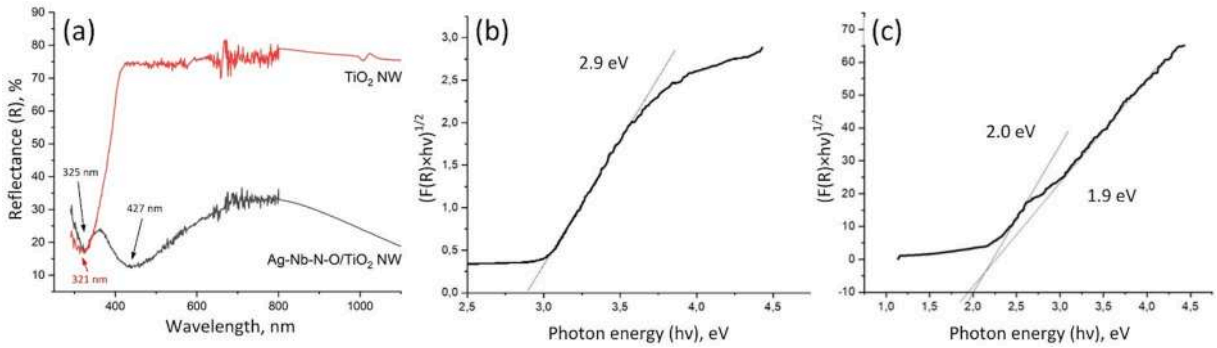

Fig. 7. Optical characterization of the samples: (a) DR spectra of TiO_2 NWs and Ag-Nb-N-O/TiO_2 NWs; (b, c) $(F(R) \times h\nu)^{1/2}$ corresponding curves.

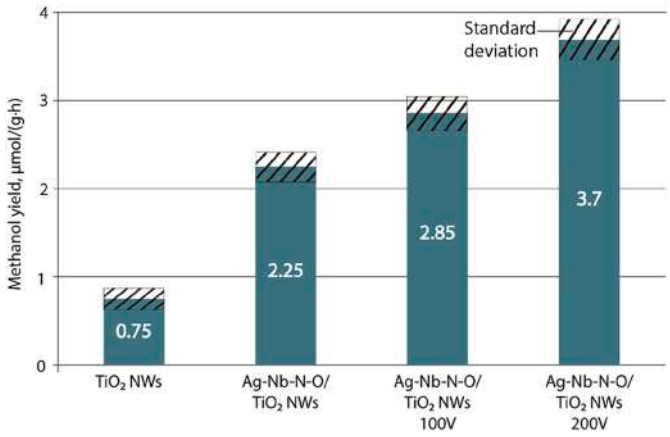

Fig. 8. Methanol yield for TiO_2 NWs and Ag-Nb-N-O/TiO_2 NWs samples at a reactor temperature of 100 °C, as well as when applying a voltage of 100 V and 200 V to the Ag-Nb-N-O/TiO_2 NWs sample.

heterojunction formation in presence of Ag, which can contribute to the photocatalytic activity in parallel to the LSPR effect.

3.6. Photocatalytic activity study

A comparative analysis of the TiO_2 NWs and Ag-Nb-N-O/TiO_2 NWs samples was carried out during experiments on photoreduction of CO_2 in the water vapor at a reactor temperature of 100 °C. The rationale for choosing the reactor temperature of 100 °C is presented in our previous paper [30], where we compared the photocatalytic activity of the synthesized TiO_2 NWs at different temperatures and explained that the best yield of products is observed at this temperature.

As a result of studying the reaction of CO_2 photoreduction in the presence of water vapor on the surface of TiO_2 NWs and Ag-Nb-N-O/TiO_2 NWs samples, it was found that the predominant reaction product is methanol, therefore the comparison was carried out based on this product. As reported in the literature [65,66] pure TiO_2 produces methanol under UV irradiation. In this case, electron-hole pairs are generated in TiO_2; the photogenerated holes oxidize adsorbed H_2O molecules on the TiO_2 surface according to reaction (2), providing H^+ for the subsequent reduction process, while the photogenerated electrons participate in the reduction of adsorbed CO_2 to methanol via reaction (3).

$$H_2O + h^+ \rightarrow H^+ + OH^- \quad (2)$$

$$CO_2 + 6H^+ + 6e^- \rightarrow CH_3OH + H_2O \quad (3)$$

Fig. 8 shows a comparative diagram with the average methanol yield as a result of CO_2 photoreduction on the surface of TiO_2 NWs and Ag-Nb-N-O/TiO_2 NWs samples with and without exposure to an electric field.

The Ag-Nb-N-O/TiO_2 NWs sample yields methanol amount tree times more compared to the TiO_2 NWs free of Ag particles. Therefore, the modification of the TiO_2 NWs with Ag particles via extrusion from the alloy film improves photocatalytic activity of the entire sample for an effective reduction of CO_2.

In this regard, a charge transfer mechanism of the Ag/TiO_2 photocatalytic activity under visible light can take a place. Many groups have accepted that the plasmon resonance excites electrons in Ag particles for their subsequent transfer to the TiO_2 conduction band. However, the surface plasmons can be imagined as a charge density wave on the surface of the metal nanostructure, i.e. the Ag particles do not have an equivalent of the highest occupied or the lowest un-occupied molecular orbital. The plasmon-induced charge located at the metal Fermi level and can hardly enable the reduction and oxidation half reactions in the same way as TiO_2 [67]. At the same time, stemming from the TEM-image we assume the Ag clusters' formation on the TiO_2 NWs surface, which analogues were reported to participate in the visible light photocatalysis [68]. Supposedly, the metal clusters have molecular-like excited-state properties that makes them photochemically active. In addition, electron transfer is possible from metal to TiO_2 nanostructures [69]. This mechanism is assisted by the surface plasmon decay that results in formation of the "hot" electron-hole pairs in metal followed by their injection in TiO_2 [70].

Even more effective photocatalytic activity is provided in accordance with the local electromagnetic field enhancement mechanism. As reported elsewhere [53], the Ag-Nb-N-O films possess a remarkable surface enhancement of Raman scattering when exposed to visible light, which wavelength coincides with the surface plasmon resonance band of Ag NPs. The numerous "hot spots" between the extruded, coalesced, and redeposited Ag particles in the annealed sample induce local charge generation in TiO_2 NWs.

The LSPR effect that occurs if the frequency of the electromagnetic field of the incident light coincides with the frequency of the electron gas oscillation in the metal is accompanied by the enormous enhancement of energy (e.g. electromagnetic field) around Ag particles. Since the quantum of collective oscillations of the electron gas – the plasmon – is an unstable quasi-particle that decays rather quickly, its energy must be converted into other forms of energy [71,72]. Therefore, the energy of the decayed plasmon is transferred to individual electrons. As a result, an electron with an excess energy becomes a 'hot electron'. Its energy can be used either for injection into the material in contact with the plasmonic nanoparticle or for initiating a separate catalytic reaction [73]. At the same time, 'hot electrons' collide with the crystal lattice of the metal, transferring energy to phonons, which leads to heating, or 'plasmon heating' [74]. These two processes – the generation of 'hot electrons' and plasmon heating – occur simultaneously, and it is practically impossible to distinguish their effects experimentally.

Thus, a significant reason for the observed increase in the photocatalytic activity of the Ag-Nb-N-O/TiO_2 NWs sample is a contribution of the Ag particle LSPR, which can, in particular, manifest itself in the form of an expansion of the spectral region of photosensitivity, local heating, and additional generation of charge carriers [57]. In addition, the formation of the Schottky barrier in the Ag/TiO_2 NWs structure helps to improve the separation of electrons and holes, which reduces their recombination [75,76].

The exposure to an electric field contributes to increasing the photocatalytic activity of the Ag-Nb-N-O/TiO_2 NWs structure. As can be seen in Fig. 8, applying 100 V increased the methanol yield efficiency by approx. 30 %, while 200 V increased it by 60 %. When an electric field is applied to the Ag-Nb-N-O/TiO_2-NWs structure, charge separation processes at the heterojunction boundary are enhanced. As it is known, the external electric field plays an important role in the control of charge transfer processes [77–79]. It not only accelerates the transfer of photogenerated electrons and holes, but also reduces the probability of their recombination, creating conditions for spatial charge separation. This, in turn, promotes more efficient cathodic and anodic reactions.

There are two important processes of photocatalytic redox reactions that include (i) generation and transport of charge carriers to the reaction site in the photocatalytic material; (ii) reaction product adsorption on and desorption from the surface of the photocatalytic material. The efficiency of these processes in TiO_2-based nanoparticles and nanocomposites is mainly determined by their phase composition and the shape/size of TiO_2 nanocrystals. Our findings showed that the TiO_2 structure acquires crystalline forms of bronzes, anatase, rutile, and their combinations depending on the processing temperature, which correlate with the results reported elsewhere [30]. Each of the TiO_2 phase forms listed has different band gaps and, as a consequence, demonstrates different photocatalytic activities. At the same time, we demonstrated that the wire-like nanocrystals (1D) of TiO_2 are more photocatalytically active compared to its nanoparticles (0D) although the specific surface area of nanoparticles exceeds that of nanowires [30]. Obviously, such an

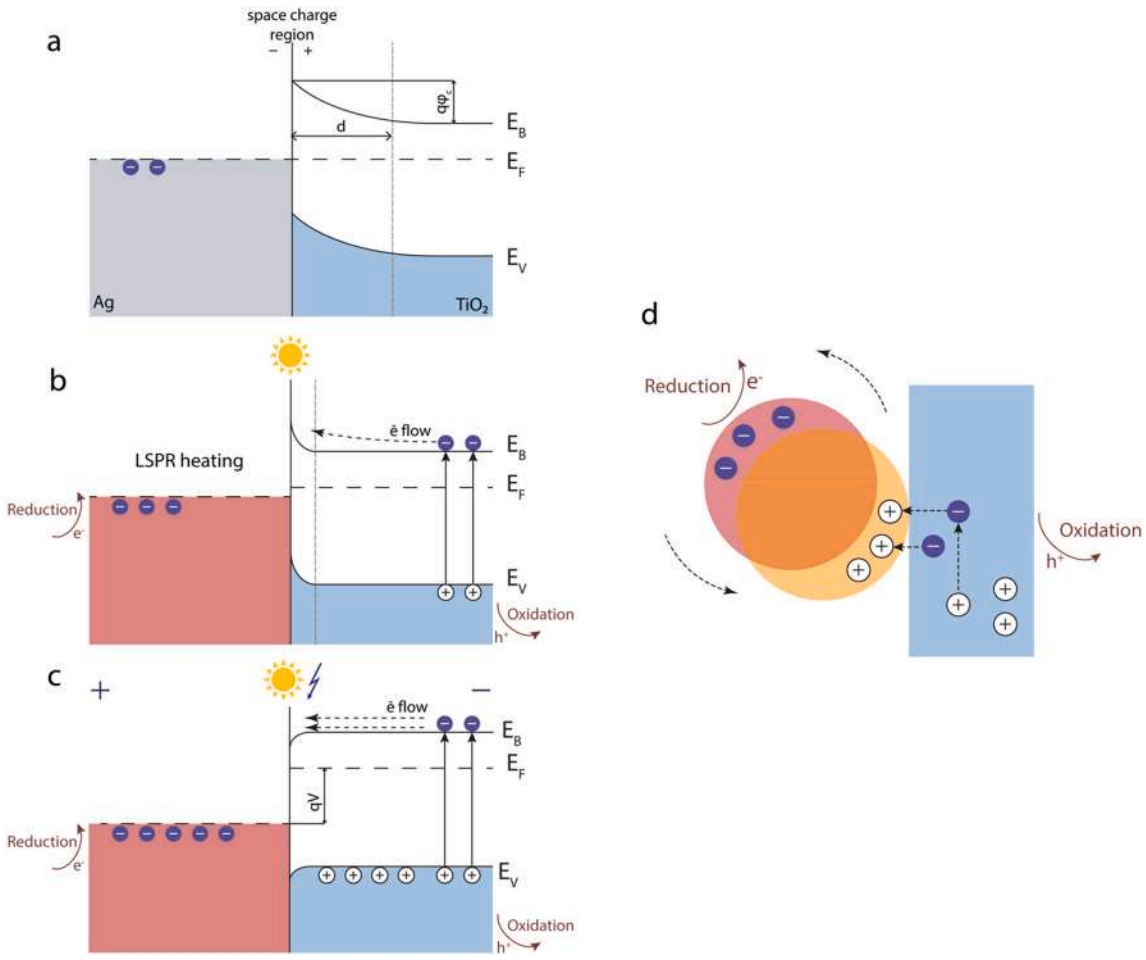

Fig. 9. Schematic representation of the charge carrier transfer in the TiO_2 NW/Ag NP heterostructure: energy band diagrams of the Ag/TiO_2 interface at the moment of (a) formation of a Schottky barrier and the barrier layer, (b) light-induced LSPR effect and the Ag NP heating, (c) applying the electric field in the forward direction to the Ag/TiO_2 Schottky contact, and (d) the consumption of electrons on the Ag NPs surface for the reduction and holes on the TiO_2 NWs surface for the oxidation. The energy-band diagrams are schematic and based on literature values of the work functions of Ag and TiO_2.

effect is directly interconnected with varied defectiveness and surface state density that affect the charge carrier mobility and recombination as well as with the number of adsorption sites per unit surface area. Furthermore, the heterostructure composed of TiO_2 and Ag NPs extruded from the Ag-Nb-N-O film possesses an increased photocatalytic activity due to the LSPR effect in the metallic nanoparticles that leads to generation of the additional hot charge carriers.

Thereby, an effective photocatalytic reduction of CO_2 on the surface of nanostructured semiconductors requires finding optimal combination of many conditions especially light exposure regimes, temperature, and gas environment composition. The excitation light source wavelength/spectral range and power defining the electric field strength manage a number of generated charge carriers, which directly participate in photocatalytic reactions. The catalyst temperature affects kinetics of precursor adsorption and reaction product desorption. Additionally, the temperature deviation increase/decrease an electrical resistivity of the photocatalyst semiconductor or, in other words, impact the charge carrier transport. The ratio of components and the composition of the gas atmosphere also affect the adsorption/desorption processes of reagents. In particular, adsorption temperature of different reagents is not the same. Thereby, an amount of some components may prevail over others on the surface of the photocatalytic material. As mentioned above, the yield of the reaction products rises proportionally to the applied electric field strength for composite photocatalytic materials. For example, this is typical for the nanocomposite of TiO_2 NWs and Ag NPs formed by heating the Ag-Nb-N-O film due to the enhancement of charge separation processes at the heterojunction boundary and more efficient transfer of photogenerated electrons and holes. In this case, a prevention of electrical breakdown or current leakage is very important because such effects lead to the localization of the electric current flow while an entire surface of the photocatalyst is inefficient in terms of the electric field contribution. An understanding of processes that occur in the TiO_2/Ag NPs heterostructure upon the light excitation and the electric field application is shown in Fig. 9.

An electrical contact between Ag NPs and TiO_2 NWs results in aligning their Fermi levels due to electron transfer from TiO_2 to Ag. As per literature data, the electron work functions for both Ag and TiO_2 can vary in the range of 4.3–4.7 eV for Ag and in the range of 4.2–4.8 eV for TiO_2 [80–83]. Therefore, we find it complicated to conclude on rectifying or non-rectifying type of the contact between Ag and TiO_2. It is generally accepted and we support this point of view based on our experimental results that at nanometer sizes the work function for Ag is over that for TiO_2 [84–86], which results in the formation of a Schottky barrier and a barrier layer at the Ag/TiO_2 interface as schematically depicted in Fig. 9 (a).

UV–vis excitation of the TiO_2 NWs/Ag NPs heterostructure induces the LSPR in Ag and simultaneously generate free charge carriers in TiO_2 due to the direct E_v-E_c transition. Moreover, the LSPR effect leads to overheating of Ag NPs, which has not been considered in discussions on the plasmon-facilitated mechanism of photocatalysis in TiO_2. Here, the fact of higher temperature in Ag NPs compared to pure TiO_2 NWs under exposure to 465 nm light (1 W LED) is confirmed by imaging the TiO_2

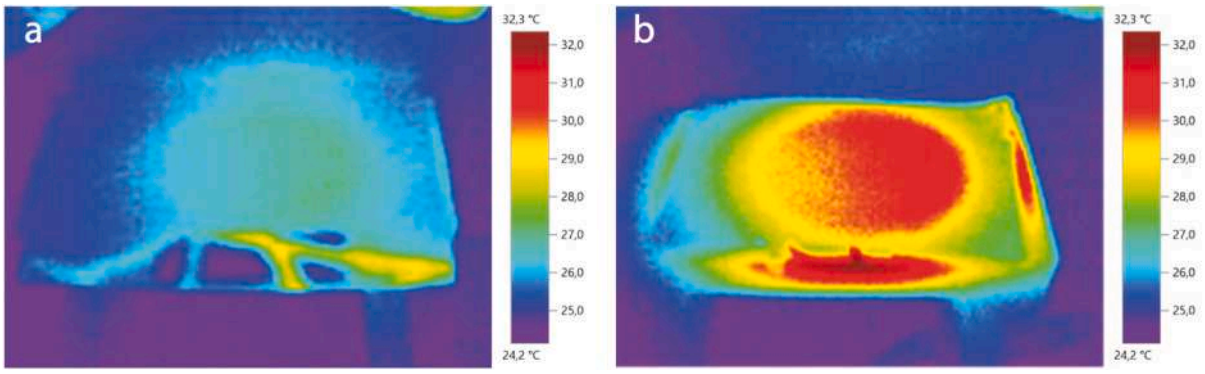

Fig. 10. IR-images of the TiO_2 NWs (a) and Ag-Nb-N-O (b) on the Ti substrate subjected to the exposure of the 465 nm LED for 2 min.

NWs and Ag-Nb-N-O layers on the Ti foil samples with IR camera, as shown in Fig. 10. The average temperatures of the irradiated regions of the TiO_2 NW and Ag-Nb-N-O/TiO_2 NW samples were 26.0 °C with the standard deviation (SD) of 0.24 and 30.2 °C with SD of 0.54 respectively. The ambient temperature during the measurements was 23.2 °C.

As a result, the Ag NP heating induces thermoelectromotive force that moves electrons in Ag and holes in TiO_2, i.e. provides the charge carrier separation. In this case, the moving plasmon in Ag NP is supposed to act as a pump, extracting electrons from TiO_2 as schematically depicted in Fig. 9(b and c). This improves efficiency of the CO_2 reduction accompanied by the consumption of electrons on the Ag NPs surface for the reduction and holes on the TiO_2 NWs surface for the oxidation (Fig. 9 (d)). Thus, the increased methanol yield observed in presence of the Ag-NPs/TiO_2-NWs heterostructure in comparison with that with the pure TiO_2-NWs is a consequence of these ongoing processes. Applying the electric field in the forward direction to the Ag/TiO_2 Schottky contact additionally enhances the charge separation process and increases the driving force of this process by qV (Fig. 9 (c)). In a course of our experiments, this suggestion was proved by an additional increase in the methanol yield when the voltage was applied.

4. Conclusions

Comparison of TiO_2 NWs and Ag-Nb-N-O/TiO_2 NWs samples shows a significant increase in photocatalytic activity in the presence of an array of Ag particles released from the Ag-Nb-N-O thin film during thermal annealing at 350 °C. Obviously, this effect can be associated with localized surface plasmon resonance in Ag particles, the formation of "hot spots" that contribute to an increase in the concentration of charge carriers (electrons and holes) participating in oxidation-reduction reactions.

Furthermore, our results demonstrate that LSPR-induced heating of Ag nanoparticles plays a crucial role in the charge carrier separation process. The temperature increase in Ag NPs, confirmed by IR imaging, generates a thermoelectromotive force that drives electron transfer from TiO_2 to Ag, thereby improving CO_2 reduction efficiency. Our finding lays the foundation for the future solving a new, non-trivial problem of experimentally determining the thermoelectromotive power, which will certainly be a continuation of this research.

In addition, the photocatalytic activity of the Ag-Nb-N-O/TiO_2 NWs structure is further enhanced under the influence of an electric field. Applying an external voltage to the Ag/TiO_2 Schottky contact intensifies charge separation and increases the driving force of electron transfer, leading to an additional rise in methanol yield. It has been shown that increasing the electric field strength contributes to an increase in the yield of methanol in the reaction of photoreduction of CO_2 in the water vapor.

Enclosing, we emphasize that our study is focused on the experimental modification, characterization, and improvement of photocatalytic activity of TiO_2 nanostructures nanomaterial, which enabled combination of LSPR, thermal effects, and electric field for enhancing CO_2 reduction efficiency. Despite the designed nanomaterial has complex variable composition that can hardly be characterized via computer simulations, our findings provided a plausible phenomenological model of coupling between LSPR-induced thermoelectromotive force and interfacial charge separation. Our approach opens a way to engineering a photocatalyst with well-controllable activity triggered by slight heating. Its successful implementation in practice strongly depends on a deeper fundamental yet research-based understanding the mechanism of the photocatalytic activity enhancement in such a system, which now is planning and requires the surface potential measurements during annealing and excitation in a reconstructed experimental setup.

Declaration of competing interest

The authors declare that they have no known competing financial interests or personal relationships that could have appeared to influence the work reported in this paper.

Acknowledgments

Sample preparation methods were developed with the support of the Russian Science Foundation Project No. 24-19-00610 (https://rscf.ru/project/24-19-00610/), and the experimental measurements were supported by the State Assignment № FSMR-2023-0003.

References

[1] A. Mills, R.H. Davies, D. Worsley, Water purification by semiconductor photocatalysis, Chem. Soc. Rev. 22 (1993) 417, https://doi.org/10.1039/cs9932200417.
[2] K. Perović, F.M. Dela Rosa, M. Kovačić, H. Kušić, U.L. Štangar, F. Fresno, D. D. Dionysiou, A. Loncaric Bozic, Recent achievements in development of TiO2-Based composite photocatalytic materials for solar driven water purification and water splitting, Materials 13 (2020) 1338, https://doi.org/10.3390/ma13061338.
[3] S.J. Armaković, M.M. Savanović, S. Armaković, Titanium dioxide as the Most used photocatalyst for water purification: an overview, Catalysts 13 (2022) 26, https://doi.org/10.3390/catal13010026.
[4] G. Pedroza-Herrera, I.E. Medina-Ramírez, J.A. Lozano-Álvarez, S.E. Rodil, Evaluation of the photocatalytic activity of copper doped TiO2 nanoparticles for the purification and/or disinfection of industrial effluents, Catal. Today 341 (2020) 37–48, https://doi.org/10.1016/j.cattod.2018.09.017.
[5] A. Pancielejko, M. Rzepnikowska, A. Zaleska-Medynska, J. Łuczak, P. Mazierski, Enhanced visible light active WO3 thin films toward air purification: effect of the synthesis conditions, Materials 13 (2020) 3506, https://doi.org/10.3390/ma13163506.
[6] M. Le Pivert, O. Kerivel, B. Zerelli, Y. Leprince-Wang, ZnO nanostructures based innovative photocatalytic road for air purification, J. Clean. Prod. 318 (2021) 128447, https://doi.org/10.1016/j.jclepro.2021.128447.
[7] A. Milionis, A. Tripathy, M. Donati, C.S. Sharma, F. Pan, K. Maniura-Weber, Q. Ren, D. Poulikakos, Water-based scalable methods for self-cleaning antibacterial ZnO-Nanostructured surfaces, Ind. Eng. Chem. Res. 59 (2020) 14323–14333, https://doi.org/10.1021/acs.iecr.0c01998.

[8] H. Liu, Y. Feng, J. Shao, Y. Chen, Z.L. Wang, H. Li, X. Chen, Z. Bian, Self-cleaning triboelectric nanogenerator based on TiO2 photocatalysis, Nano Energy 70 (2020) 104499, https://doi.org/10.1016/j.nanoen.2020.104499.

[9] S. Adhikari, K. Sarath Chandra, D.-H. Kim, G. Madras, D. Sarkar, Understanding the morphological effects of WO 3 photocatalysts for the degradation of organic pollutants, Adv. Powder Technol. 29 (2018) 1591–1600, https://doi.org/10.1016/j.apt.2018.03.024.

[10] Y. Zhang, N. Zhang, T. Wang, H. Huang, Y. Chen, Z. Li, Z. Zou, Heterogeneous degradation of organic contaminants in the photo-Fenton reaction employing pure cubic β-Fe2O3, Appl. Catal. B Environ. 245 (2019) 410–419, https://doi.org/10.1016/j.apcatb.2019.01.003.

[11] C. Cao, B. Zhang, S. Lin, p-type ZnO for photocatalytic water splitting, APL Mater. 10 (2022) 030901, https://doi.org/10.1063/5.0083753.

[12] T. Liu, Y. Wang, P. Shan, Y. Chen, X. Zhao, W. Tian, Y. Zhang, R. Feng, H. Yuan, H. Cui, Hydrogen evolution from MoSe2/WO3(0 0 1) heterojunction by photocatalytic water splitting: a density functional theory study, Appl. Surf. Sci. 564 (2021) 150117, https://doi.org/10.1016/j.apsusc.2021.150117.

[13] Y. Feng, C. Wang, P. Cui, C. Li, B. Zhang, L. Gan, S. Zhang, X. Zhang, X. Zhou, Z. Sun, K. Wang, Y. Duan, H. Li, K. Zhou, H. Huang, A. Li, C. Zhuang, L. Wang, Z. Zhang, X. Han, Ultrahigh photocatalytic CO_2 reduction efficiency and selectivity manipulation by single-tungsten-atom oxide at the atomic step of TiO_2, Adv. Mater. 34 (2022) 2109074, https://doi.org/10.1002/adma.202109074.

[14] G. Chen, Z. Zhou, B. Li, X. Lin, C. Yang, Y. Fang, W. Lin, Y. Hou, G. Zhang, S. Wang, S-scheme heterojunction of crystalline carbon nitride nanosheets and ultrafine WO3 nanoparticles for photocatalytic CO2 reduction, Journal of Environmental Sciences 140 (2024) 103–112, https://doi.org/10.1016/j.jes.2023.05.028.

[15] L. Wang, H. Tan, L. Zhang, B. Cheng, J. Yu, In-situ growth of few-layer graphene on ZnO with intimate interfacial contact for enhanced photocatalytic CO2 reduction activity, Chem. Eng. J. 411 (2021) 128501, https://doi.org/10.1016/j.cej.2021.128501.

[16] J. Tian, Z. Zhao, A. Kumar, R.I. Boughton, H. Liu, Recent progress in design, synthesis, and applications of one-dimensional TiO_2 nanostructured surface heterostructures: a review, Chem. Soc. Rev. 43 (2014) 6920–6937, https://doi.org/10.1039/C4CS00180J.

[17] C.L. Bianchi, S. Gatto, C. Pirola, A. Naldoni, A. Di Michele, G. Cerrato, V. Crocellà, V. Capucci, Photocatalytic degradation of acetone, acetaldehyde and toluene in gas-phase: Comparison between nano and micro-sized TiO2, Appl. Catal. B Environ. 146 (2014) 123–130, https://doi.org/10.1016/j.apcatb.2013.02.047.

[18] S.M. Tichapondwa, J.P. Newman, O. Kubheka, Effect of TiO2 phase on the photocatalytic degradation of methylene blue dye, Phys. Chem. Earth, Parts A/B/C 118–119 (2020) 102900, https://doi.org/10.1016/j.pce.2020.102900.

[19] A.M. Luís, M.C. Neves, M.H. Mendonça, O.C. Monteiro, Influence of calcination parameters on the TiO2 photocatalytic properties, Mater. Chem. Phys. 125 (2011) 20–25, https://doi.org/10.1016/j.matchemphys.2010.08.019.

[20] R. Qian, H. Zong, J. Schneider, G. Zhou, T. Zhao, Y. Li, J. Yang, D.W. Bahnemann, J.H. Pan, Charge carrier trapping, recombination and transfer during TiO2 photocatalysis: an overview, Catal. Today 335 (2019) 78–90, https://doi.org/10.1016/j.cattod.2018.10.053.

[21] K. Ozawa, S. Yamamoto, K. Mase, I. Matsuda, A surface science approach to unveiling the TiO_2 photocatalytic mechanism: correlation between photocatalytic activity and carrier lifetime, E-J, Surf. Sci. Nanotechnol. 17 (2019) 130–147, https://doi.org/10.1380/ejssnt.2019.130.

[22] N. Thakur, N. Thakur, K. Kumar, Phytochemically and PVP stabilized TiO2 nanospheres for enhanced photocatalytic and antioxidant efficiency, Mater. Today Commun. 35 (2023) 105587, https://doi.org/10.1016/j.mtcomm.2023.105587.

[23] S. Zhang, L. Zhao, B. Huang, X. Li, Enhanced sensing performance of Au-decorated TiO2 nanospheres with hollow structure for formaldehyde detection at room temperature, Sensor. Actuator. B Chem. 358 (2022) 131465, https://doi.org/10.1016/j.snb.2022.131465.

[24] S. Hoang, Y. Guo, A.J. Binder, W. Tang, S. Wang, J. Liu, H. Tran, X. Lu, Y. Wang, Y. Ding, E.A. Kyriakidou, J. Yang, T.J. Toops, T.R. Pauly, R. Ramprasad, P.-X. Gao, Activating low-temperature diesel oxidation by single-atom Pt on TiO2 nanowire array, Nat. Commun. 11 (2020) 1062, https://doi.org/10.1038/s41467-020-14816-w.

[25] Y. Feng, H.H.M. Rijnaarts, D. Yntema, Z. Gong, D.D. Dionysiou, Z. Cao, S. Miao, Y. Chen, Y. Ye, Y. Wang, Applications of anodized TiO2 nanotube arrays on the removal of aqueous contaminants of emerging concern: a review, Water Res. 186 (2020) 116327, https://doi.org/10.1016/j.watres.2020.116327.

[26] Y. Wang, Y. Zhang, X. Zhu, Y. Liu, Z. Wu, Fluorine-induced oxygen vacancies on TiO2 nanosheets for photocatalytic indoor VOCs degradation, Appl. Catal. B Environ. 316 (2022) 121610, https://doi.org/10.1016/j.apcatb.2022.121610.

[27] M. Ge, C. Cao, J. Huang, S. Li, Z. Chen, K.-Q. Zhang, S.S. Al-Deyab, Y. Lai, A review of one-dimensional TiO_2 nanostructured materials for environmental and energy applications, J. Mater. Chem. A 4 (2016) 6772–6801, https://doi.org/10.1039/C5TA09323F.

[28] M. Adachi, Y. Murata, J. Takao, J. Jiu, M. Sakamoto, F. Wang, Highly efficient dye-sensitized solar cells with a titania thin-film electrode composed of a network structure of single-crystal-like TiO_2 nanowires made by the "Oriented Attachment" mechanism, J. Am. Chem. Soc. 126 (2004) 14943–14949, https://doi.org/10.1021/ja048068s.

[29] S. Huang, D.S. Kilin, Anatase TiO_2 nanowires, thin films, and surfaces: ab initio studies of electronic properties and non-adiabatic excited state dynamics, MRS Proc 1659 (2014) 129–134, https://doi.org/10.1557/opl.2014.354.

[30] A.M. Tarasov, L.I. Sorokina, D.A. Dronova, O. Volovlikova, A.Yu Trifonov, S. S. Itskov, A.V. Tregubov, E.N. Shabaeva, E.S. Zhurina, S.V. Dubkov, D.V. Kozlov, D. Gromov, Influence of the structure of hydrothermal-synthesized TiO2 nanowires formed by annealing on the photocatalytic reduction of CO2 in H2O vapor, Nanomaterials 14 (2024) 1370, https://doi.org/10.3390/nano14161370.

[31] W. Jiang, S. Bai, L. Wang, X. Wang, L. Yang, Y. Li, D. Liu, X. Wang, Z. Li, J. Jiang, Y. Xiong, Integration of multiple plasmonic and Co-Catalyst nanostructures on TiO_2 nanosheets for visible-near-infrared photocatalytic hydrogen evolution, Small 12 (2016) 1640–1648, https://doi.org/10.1002/smll.201503552.

[32] A. Meng, L. Zhang, B. Cheng, J. Yu, Dual cocatalysts in TiO_2 photocatalysis, Adv. Mater. 31 (2019) 1807660, https://doi.org/10.1002/adma.201807660.

[33] H. He, Y. Ren, Y.-H. Zhu, R. Peng, S. Lan, J. Zhou, B. Yang, Y. Si, N. Li, Continuous flow photothermal catalytic CO_2 reduction: materials, mechanisms, and system design, ACS Catal. 15 (2025) 10480–10520, https://doi.org/10.1021/acscatal.5c02269.

[34] P. Wang, B. Huang, Y. Dai, M.-H. Whangbo, Plasmonic photocatalysts: harvesting visible light with noble metal nanoparticles, Phys. Chem. Chem. Phys. 14 (2012) 9813, https://doi.org/10.1039/c2cp40823f.

[35] C. Liu, H. Dong, N. Wu, Y. Cao, X. Zhang, Plasmonic resonance energy transfer enhanced photodynamic therapy with Au@SiO_2 @Cu_2 O/Perfluorohexane nanocomposites, ACS Appl. Mater. Interfaces 10 (2018) 6991–7002, https://doi.org/10.1021/acsami.8b00112.

[36] Y. Ren, Y. Si, M. Du, C. You, C. Zhang, Y. Zhu, Z. Sun, K. Huang, M. Liu, L. Duan, N. Li, Photothermal synergistic effect induces bimetallic cooperation to modulate product selectivity of CO_2 reduction on different CeO_2 crystal facets, Angew. Chem. Int. Ed. 63 (2024) e202410474, https://doi.org/10.1002/anie.202410474.

[37] A. Wang, X. Kong, Review of recent progress of plasmonic materials and nano-structures for surface-enhanced raman scattering, Materials 8 (2015) 3024–3052, https://doi.org/10.3390/ma8063024.

[38] S. Linic, P. Christopher, D.B. Ingram, Plasmonic-metal nanostructures for efficient conversion of solar to chemical energy, Nature Mater 10 (2011) 911–921, https://doi.org/10.1038/nmat3151.

[39] S.G. Kumar, L.G. Devi, Review on modified TiO_2 photocatalysis under UV/Visible light: selected results and related mechanisms on interfacial charge carrier transfer dynamics, J. Phys. Chem. A 115 (2011) 13211–13241, https://doi.org/10.1021/jp204364a.

[40] J.S. DuChene, B.C. Sweeny, A.C. Johnston-Peck, D. Su, E.A. Stach, W.D. Wei, Prolonged hot electron dynamics in Plasmonic-Metal/Semiconductor heterostructures with implications for solar photocatalysis, Angew. Chem. Int. Ed. 53 (2014) 7887–7891, https://doi.org/10.1002/anie.201404259.

[41] D.G. Gromov, S.V. Dubkov, A.I. Savitskiy, YuP. Shaman, A.A. Polokhin, I. A. Belogorokhov, A.Yu Trifonov, Optimization of nanostructures based on Au, Ag, Au Ag nanoparticles formed by thermal evaporation in vacuum for SERS applications, Appl. Surf. Sci. 489 (2019) 701–707, https://doi.org/10.1016/j.apsusc.2019.05.286.

[42] R. Li, C. Pang, Z. Li, F. Chen, Plasmonic nanoparticles in dielectrics synthesized by ion beams: optical properties and photonic applications, Adv. Opt. Mater. 8 (2020) 1902087, https://doi.org/10.1002/adom.201902087.

[43] W. Liu, J. Wang, X. Xu, C. Zhao, X. Xu, P.S. Weiss, Single-step dual-layer photolithography for tunable and scalable nanopatterning, ACS Nano 15 (2021) 12180–12188, https://doi.org/10.1021/acsnano.1c03703.

[44] A. Dolgyi, H. Bandarenka, S. Prischepa, K. Yanushkevich, P. Nenzi, M. Balucani, V. Bondarenko, Electrochemical deposition of Ni into mesoporous silicon, ECS Trans. 41 (2012) 111–118, https://doi.org/10.1149/1.3699385.

[45] E.B. Chubenko, S.V. Redko, A.I. Sherstnyov, V.A. Petrovich, D.A. Kotov, V. P. Bondarenko, Influence of the surface layer on the electrochemical deposition of metals and semiconductors into mesoporous silicon, Semiconductors 50 (2016) 372–376, https://doi.org/10.1134/S1063782616030040.

[46] A.Yu Panarin, S.N. Terekhov, K.I. Kholostov, V.P. Bondarenko, SERS-active substrates based on n-type porous silicon, Appl. Surf. Sci. 256 (2010) 6969–6976, https://doi.org/10.1016/j.apsusc.2010.05.008.

[47] H. Bandarenka, S. Redko, P. Nenzi, M. Balucani, M. Balucani, Optimization of chemical displacement deposition of copper on porous silicon, J. Nanosci. Nanotechnol. 12 (2012) 8725–8731, https://doi.org/10.1166/jnn.2012.6470.

[48] C. Fernández-Lodeiro, J. Fernández-Lodeiro, E. Carbó-Argibay, C. Lodeiro, J. Pérez-Juste, I. Pastoriza-Santos, The versatility of Fe(II) in the synthesis of uniform citrate-stabilizedplasmonic nanoparticles with tunable size at room temperature, Nano Res. 13 (2020) 2351–2355, https://doi.org/10.1007/s12274-020-2854-1.

[49] J.L. Cholula-Díaz, D. Lomelí-Marroquín, B. Pramanick, A. Nieto-Argüello, L. A. Cantú-Castillo, H. Hwang, Synthesis of colloidal silver nanoparticle clusters and their application in ascorbic acid detection by SERS, Colloids Surf. B Biointerfaces 163 (2018) 329–335, https://doi.org/10.1016/j.colsurfb.2017.12.051.

[50] G. Lin, W. Lu, W. Cui, L. Jiang, A simple synthesis method for gold Nano- and microplate fabrication using a tree-type multiple-amine head surfactant, Cryst. Growth Des. 10 (2010) 1118–1123, https://doi.org/10.1021/cg9008976.

[51] M.R. El-Zahry, I.H. Refaat, H.A. Mohamed, B. Lendl, Sequential SERS determination of aspirin and vitamin C using in situ laser-induced photochemical silver substrate synthesis in a moving flow cell, Anal. Bioanal. Chem. 408 (2016) 4733–4741, https://doi.org/10.1007/s00216-016-9562-4.

[52] X. Lian, H. Sun, Y. Lv, G. Wang, Room temperature self-assembled Ag nanoparticles/Mo-37.5% Ag film as efficient flexible SERS substrate, Mater. Lett. 275 (2020) 128164, https://doi.org/10.1016/j.matlet.2020.128164.

[53] S.V. Dubkov, D.V. Novikov, H.V. Bandarenka, A.A. Burko, A.Y. Trifonov, L. S. Volkova, P.A. Edelbekova, E.A. Lebedev, E.A. Skryleva, D.G. Gromov, Express formation and characterization of SERS-active substrate from a non-degradable Ag-Nb-N-O film, Appl. Surf. Sci. 645 (2024) 158682, https://doi.org/10.1016/j.apsusc.2023.158682.

[54] C.O.W. Trost, A. Lassnig, P. Kreiml, T. Jörg, V.L. Terziyska, Christian Mitterer, M. J. Cordill, Enthalpy-driven self-healing in thin metallic films on flexible substrates, Adv. Mater. 36 (2024) 2401007, https://doi.org/10.1002/adma.202401007.
[55] S. Li, S. Liang, H. Zhang, P. Shi, H. Zheng, M. Shen, Y. Lv, H. Sun, G. Wang, Spontaneously formed dense Cu nanoislands and superior SERS properties of Cu nanoislands/Cu-Ta-Mo films, Surf. Interfaces 46 (2024) 104132, https://doi.org/10.1016/j.surfin.2024.104132.
[56] O. Shtyka, R. Ciesielski, A. Kedziora, S. Dubkov, D. Gromov, M. Zakrzewski, T. Maniecki, Catalytic activity of semiconductors under the influence of electric fields, Appl. Catal. Gen. 635 (2022) 118541, https://doi.org/10.1016/j.apcata.2022.118541.
[57] Y. Xu, Z. Zhou, M. Zou, Y. Liu, Y. Zheng, Y. Yang, S. Lan, J. Lan, C.-W. Nan, Y.-H. Lin, Multi-field driven hybrid catalysts for CO2 reduction: progress, mechanism and perspective, Mater. Today 54 (2022) 225–246, https://doi.org/10.1016/j.mattod.2022.02.005.
[58] K.N. Tu, Erratum: shallow and parallel silicide contacts, J. Vac. Sci. Technol. 19 (1982) 766, https://doi.org/10.1116/1.571686. Journal of Vacuum Science and Technology 21 (1982) 100–100.
[59] D.G. Gromov, A.I. Mochalov, V.P. Pugachevich, I.N. Sorokin, Interaction between binary alloy thin films and silicon substrate: the conditions of bilayer formation and the effect of additional component, Appl. Phys. Mater. Sci. Process 70 (2000) 333–340, https://doi.org/10.1007/s003390050056.
[60] P. Mierczynski, S.V. Dubkov, S.V. Bulyarskii, A.A. Pavlov, S.N. Skorik, A. Y. Trifonov, A. Mierczynska, E.P. Kitsyuk, S.A. Gavrilov, T.P. Maniecki, D. G. Gromov, Growth of carbon nanotube arrays on various CtMe alloy films by chemical vapour deposition method, J. Mater. Sci. Technol. 34 (2018) 472–480, https://doi.org/10.1016/j.jmst.2017.01.030.
[61] E.P. Kitsyuk, D.G. Gromov, E.N. Redichev, I.V. Sagunova, Specifics of low-temperature melting and disintegration into drops of silver thin films, Prot Met Phys Chem Surf 48 (2012) 304–309, https://doi.org/10.1134/S2070205112030094.
[62] YuYa Gafner, D.G. Gromov, R.L. Volkov, S.V. Dubkov, D.A. Ryzhkova, S.L. Gafner, A.A. Cherepovskaya, D.V. Novikov, T.S. Grishin, N.I. Borgardt, Mechanisms of Au and Ag nanoparticle array evolution studied by in-situ TEM and molecular dynamics simulation, Surf. Interfaces 54 (2024) 105165, https://doi.org/10.1016/j.surfin.2024.105165.
[63] G. Sanzone, M. Zimbone, G. Cacciato, F. Ruffino, R. Carles, V. Privitera, M. G. Grimaldi, Ag/TiO2 nanocomposite for visible light-driven photocatalysis, Superlattice. Microst. 123 (2018) 394–402, https://doi.org/10.1016/j.spmi.2018.09.028.
[64] S. Landi, I.R. Segundo, C. Afonso, O. Lima, M.F.M. Costa, E. Freitas, J. Carneiro, Evaluation of band gap energy of TiO2 precipitated from titanium sulphate, Phys. B Condens. Matter 639 (2022) 414008, https://doi.org/10.1016/j.physb.2022.414008.
[65] T. Qu, S. Wei, Z. Xiong, J. Zhang, Y. Zhao, Progress and prospect of CO2 photocatalytic reduction to methanol, Fuel Process. Technol. 251 (2023) 107933, https://doi.org/10.1016/j.fuproc.2023.107933.
[66] T.P. Nguyen, D.L.T. Nguyen, V.-H. Nguyen, T.-H. Le, D.-V.N. Vo, Q.T. Trinh, S.-R. Bae, S.Y. Chae, S.Y. Kim, Q.V. Le, Recent advances in TiO2-Based photocatalysts for reduction of CO2 to fuels, Nanomaterials 10 (2020) 337, https://doi.org/10.3390/nano10020337.
[67] W. Hou, S.B. Cronin, A review of surface plasmon resonance-enhanced photocatalysis, Adv Funct Materials 23 (2013) 1612–1619, https://doi.org/10.1002/adfm.201202148.
[68] W.-T. Chen, Y.-J. Hsu, P.V. Kamat, Realizing visible photoactivity of metal nanoparticles: Excited-State behavior and electron-transfer properties of silver (Ag_8) clusters, J. Phys. Chem. Lett. 3 (2012) 2493–2499, https://doi.org/10.1021/jz300940c.
[69] A. Furube, L. Du, K. Hara, R. Katoh, M. Tachiya, Ultrafast plasmon-induced electron transfer from gold nanodots into TiO_2 nanoparticles, J. Am. Chem. Soc. 129 (2007) 14852–14853, https://doi.org/10.1021/ja076134v.
[70] S. Mubeen, G. Hernandez-Sosa, D. Moses, J. Lee, M. Moskovits, Plasmonic photosensitization of a wide band gap semiconductor: converting plasmons to charge carriers, Nano Lett. 11 (2011) 5548–5552, https://doi.org/10.1021/nl203457v.
[71] J.G. Liu, H. Zhang, S. Link, P. Nordlander, Relaxation of plasmon-induced hot carriers, ACS Photonics 5 (2018) 2584–2595, https://doi.org/10.1021/acsphotonics.7b00881.
[72] H. Lee, Y. Park, K. Song, J.Y. Park, Surface plasmon-induced hot carriers: generation, detection, and applications, Acc. Chem. Res. 55 (2022) 3727–3737, https://doi.org/10.1021/acs.accounts.2c00623.
[73] L. Mascaretti, A. Naldoni, Hot electron and thermal effects in plasmonic photocatalysis, J. Appl. Phys. 128 (2020) 041101, https://doi.org/10.1063/5.0013945.
[74] A.O. Govorov, H.H. Richardson, Generating heat with metal nanoparticles, Nano Today 2 (2007) 30–38, https://doi.org/10.1016/S1748-0132(07)70017-8.
[75] N.L.H. Hoang, M.Q. Luu, V.T. Pham, M.H. Nguyen, T.L. Nguyen, T.H. Pham, C. H. Hoang, H.L. Nguyen, Influence of Ag on the properties of Ag combined Nb-doped TiO2 (TNO) thin films deposited by a co-sputtering process, Indian J. Phys. 92 (2018) 1413–1418, https://doi.org/10.1007/s12648-018-1245-x.
[76] S. Liu, Q. Zhou, D. Wen, C. Wu, Y. Pan, X. Liu, Z. Huang, N. Li, Particle size-dependent charge transfer dynamics for boosting CO_2 photoreduction over Ag/TiO_2 heterojunction, ACS Catal. 14 (2024) 8105–8115, https://doi.org/10.1021/acscatal.4c01544.
[77] K.MdR. Karim, M. Tarek, ShaheenM. Sarkar, R. Mouras, H.R. Ong, H. Abdullah, C. K. Cheng, MdM.R. Khan, Photoelectrocatalytic reduction of CO2 to methanol over CuFe2O4@PANI photocathode, Int. J. Hydrogen Energy 46 (2021) 24709–24720, https://doi.org/10.1016/j.ijhydene.2020.02.195.
[78] Y. Song, W. Chen, W. Wei, Y. Sun, Advances in clean fuel ethanol production from Electro-, Photo- and photoelectro-catalytic CO2 reduction, Catalysts 10 (2020) 1287, https://doi.org/10.3390/catal10111287.
[79] M.N. Tran, M. Moreau, A. Addad, A. Teurtrie, T. Roland, V. De Waele, M. Dewitte, L. Thomas, G. Levêque, C. Dong, P. Simon, K. Ben Tayeb, D. Mele, V. Ordomsky, B. Grandidier, Boosting gas-phase TiO_2 photocatalysis with weak electric field strengths of Volt/Centimeter, ACS Appl. Mater. Interfaces 16 (2024) 14852–14863, https://doi.org/10.1021/acsami.3c19031.
[80] S. Kashiwaya, J. Morasch, V. Streibel, T. Toupance, W. Jaegermann, A. Klein, The work function of TiO2, Surfaces 1 (2018) 73–89, https://doi.org/10.3390/surfaces1010007.
[81] D. Das, S. Shyam, Reduced work function in anatase ⟨101⟩ TiO_2 films self-doped by O-Vacancy-Dependent Ti^{3+} bonds controlling the photocatalytic dye degradation performance, Langmuir 40 (2024) 10502–10517, https://doi.org/10.1021/acs.langmuir.4c00028.
[82] R. Sellappan, M.G. Nielsen, F. González-Posada, P.C.K. Vesborg, I. Chorkendorff, D. Chakarov, Effects of plasmon excitation on photocatalytic activity of Ag/TiO2 and Au/TiO2 nanocomposites, J. Catal. 307 (2013) 214–221, https://doi.org/10.1016/j.jcat.2013.07.024.
[83] V. Mansfeldova, M. Zlamalova, H. Tarabkova, P. Janda, M. Vorokhta, L. Piliai, L. Kavan, Work function of TiO_2 (Anatase, rutile, and brookite) single crystals: effects of the environment, J. Phys. Chem. C 125 (2021) 1902–1912, https://doi.org/10.1021/acs.jpcc.0c10519.
[84] Y. Wang, L. Liu, L. Xu, C. Meng, W. Zhu, Ag/TiO2 nanofiber heterostructures: highly enhanced photocatalysts under visible light, J. Appl. Phys. 113 (2013) 174311, https://doi.org/10.1063/1.4803844.
[85] P. Wang, D. Tanaka, S. Ryuzaki, S. Araki, K. Okamoto, K. Tamada, Silver nanoparticles with tunable work functions, Appl. Phys. Lett. 107 (2015) 151601, https://doi.org/10.1063/1.4933253.
[86] M. Schnippering, M. Carrara, A. Foelske, R. Kötz, D.J. Fermín, Electronic properties of Ag nanoparticle arrays. A Kelvin probe and high resolution XPS study, Phys. Chem. Chem. Phys. 9 (2007) 725–730, https://doi.org/10.1039/B611496B.